Materials Science and Engineering C 61 (2016) 506–515

Contents lists available at ScienceDirect

Materials Science and Engineering C

journal homepage: www.elsevier.com/locate/msec

A sensitive DNA biosensor fabricated from gold nanoparticles and graphene oxide on a glassy carbon electrode

Saeedeh Hajihosseini [a], Navid Nasirizadeh [b,*], Mohammad Saeid Hejazi [c], Parichereh Yaghmaei [a]

[a] Department of Biology, Science and Research Branch, Islamic Azad University, Tehran, Iran
[b] Department of Textile and Polymer Engineering, Yazd Branch, Islamic Azad University, Yazd, Iran
[c] Faculty of Pharmacy, Tabriz University of Medical Sciences, Tabriz, Iran

ARTICLE INFO

Article history:
Received 22 July 2015
Received in revised form 14 December 2015
Accepted 28 December 2015
Available online 31 December 2015

Keywords:
DNA biosensor
Helicobacter pylori
Oracet blue
Electrochemical method

ABSTRACT

A sensitive electrochemical DNA biosensor was developed for *Helicobacter pylori* (*H. pylori*) detection using differential pulse voltammetry. Single-stranded DNA probe was immobilized on a graphene oxide/gold nanoparticles modified glassy carbon electrode (GO/AuNP$_s$/GCE). A hybridization reaction was conducted with the target DNA and the immobilized DNA on the electrode surface. Oracet blue (OB) was selected for the first time as a redox indicator for amplifying the electrochemical signal of DNA.

Enhanced sensitivity was achieved through combining the excellent electric conductivity of GO/AuNPs and the electroactivity of the OB. The DNA biosensor displayed excellent performance to demonstrate the differences between the voltammetric signals of the OB obtained from different hybridization samples (non-complementary, mismatch and complementary DNAs). The proposed biosensor has a linear range of 60.0–600.0 pM and a detection limit of 27.0 pM for detection of *H. pylori*. In addition, the biosensor have responded very well in the simulated real sample evaluations, signifying its potential to be used in future clinical detection of the *H. pylori* bacteria.

1. Introduction

It has been demonstrated that *Helicobacter pylori* (*H. pylori*) is one of the most common bacterial infections in humans and the etiologic agent of a majority of upper gastro duodenal diseases [1]. Nowadays, *H. pylori* is firmly established as the etiologic agent of acute or chronic gastritis and as a major risk factor for peptic ulcer disease and the B-cell mucosa-associated lymphoid tissue (MALT) lymphoma [2]. It is currently known that infection with *H. pylori* is the primary identified cause of gastric cancer. As for the relationship between *H. pylori* and peptic ulcer disease, gastric cancer [3], there is an urgent need for new strategies to prevent the spread of this bacterium.

Different strategies have been used for detection of *H. pylori*, including fluorescence techniques [6], mass spectroscopy [4,5], hematoxylin and eosin (H&E) stain, Giemsa stain [3], surface plasmon resonance spectroscopy [7], polymerase chain reaction [9,10] and electrochemical methods [8]. Currently, there is much interest taken in developing electrochemical DNA biosensors for rapid and specific diagnosis of bacterial and viral infections as well as genetic diseases.

Besides, various nanostructures such as gold and silver nanoparticles and carbon derivatives (i.e. carbon nanotubes (CNTs), carbon nanofibers, graphene and graphene oxide (GO) nanosheets) [11–13] have been utilized to increase performance of DNA biosensors in terms of amplification electroactivity, effective electrode surface area, etc. [14,15]. For example, to detect human hepatitis B viruses, Niu et al. [16] used silver nanoparticles and multi-walled carbon nanotubes (Ag/MWCNTs) modified glassy carbon electrode (GCE). Also, Zhang et al. [17] applied poly (3-aminobenzoicacid)-walled carbon nanotubes (PABA–MWNTs) composite films and gold nanoparticles to fabricate DNA biosensors. Xiaowei et al. [18] fabricated an electrochemical sensor using gold nanorods decorated with graphene oxide sheets for detection of DNA. Huang et al. [19] designed a new DNA biosensor based on graphene/Au nanorods/polythionine for human papillomavirus DNA detection. Furthermore, Shakuri et al. [20] made use of gold nanorods to detect hepatitis B virus.

However, Au/GO has attracted more attention than other nanostructures because they have a large surface area, excellent biocompatibility, and very high electrical conductivity, high water-solubility, and can be easily prepared via the electrostatic self-assembly technique. In addition, several manuscripts which were published previously, have utilized of the stepwise modification method using GO sheets and then assembling of AuNPs on the GO sheets [21].

* Corresponding author.
E-mail address: nasirizadeh@iauyazd.ac.ir (N. Nasirizadeh).

http://dx.doi.org/10.1016/j.msec.2015.12.091
0928-4931/

The major function of DNA biosensors is to measure the signals of DNA hybridization process. The hybridization of the probe to the target sequence can be detected using appropriate hybridization indicators [22].

Oracet blue (OB) is an anthraquinone derivative which can be assumed as a quinine. It is established that anthraquinone derivatives can be quite active in the electrocatalytic redox reactions of different analyses [23]. We have recently studied the electrochemical properties of OB modified electrodes and their application as sensors to detect hydroxylamine [23] and simultaneous determination of dopamine, ascorbic acid and uric acid [24].

In this research, a new DNA biosensor has been developed based on modified GCE with AuNPs/GO for detection of 18-mer oligonucleotides of *H. pylori*. The self-assembled monolayer (SAM) technique was applied to fabricate a recognition interface using an alkanethiol single strand DNA (ssDNA). OB served firstly as an electroactive label for the hybridization signal. Differential pulse voltammetry (DPV) was used to study the interaction of DNA with OB as well as to detect complementary, non-complementary and mismatch target DNA chains in the hybridization process.

2. Experimental

2.1. Materials

OB and other chemical reagents including K_2HPO_4, KH_2PO_4, NaCl, KCl, NaOH, HCl and absolute ethanol were purchased from Merck Company. 6-Mercapto-1-hexanol (MCH) was supplied from Aldrich. AuNPs and graphene oxide (GO) dispersion were obtained from SIGMA ALDRICH. The solutions were prepared with double distilled water. All the chemicals were used without further purification.

DNA oligonucleotides were supplied (as a lyophilized powder) from Eurofins MWG Operon with the following sequences: Thiolated DNA probe (*H. pylori*): 5′-HS (CH_2)6 AGA CAT GCA AAA AGG TAT-3′. Complementary target DNA (*H. pylori*): 5′-ATA CCT TTT TGC ATG TCT-3′, Non-complementary DNA: 5′-GAA TAT GAT TTA CAG TTT ATT TTT-3′ and mismatch 5′-ATA CCT TTT TGG ATG TCT-3′. The stock solutions of the oligonucleotides (100.0 μM) were prepared with a 10.0 mM Tris–HCl buffer (pH 8.0) containing 1.0 mM of EDTA. The stock solutions were kept frozen at −20 °C. The immobilization and hybridization solutions were a 1.0 M phosphate buffer (pH 4.5) and a 0.05 M phosphate buffer (pH 7.0) containing 0.3 M of NaCl. The washing solution was also a 0.05 M phosphate buffer (pH 7.0) containing 0.3 M of NaCl. A stock solution of 1.0 mM of OB was prepared using a 0.1 M phosphate buffer solution at the pH of 7.0. The pH was adjusted with either NaOH or H_3PO_4 solutions.

2.2. Instrumentation

Electrochemical measurements were performed with an Autolab potentiostat/galvanostat model PGSTAT 30 (EcoChemic, Utrecht, Netherlands) and a GPES 4.9 software at laboratory temperature (25 ± 1 °C). A three-electrode system was used for electrochemical experiments, involving a glassy carbon electrode (GCE) (with a surface area of 0.0314 cm^2) as the working electrode, a saturated calomel electrode (SCE) as the reference electrode, and a platinum electrode as the auxiliary electrode. All the potentials in the text were reported with respect to the reference electrode. The pH measurements were done with a Metrohm model 691 pH/mV meter. The morphology of AuNPs and GO were investigated by scanning electron microscopy (SEM) using a MIRA3 TESCAN microscope and also AuNPs were characterized by a UV–vis absorption spectrophotometer (Cary 100 spectrophotometry) and transmission electron microscopy images were recorded on a TE 2000 Ziess TEM.

2.3. Preparation of a probe-modified electrode and DNA hybridization

Prior to each measurement, the surface of a GCE was polished with a 0.05 μm alumina-water slurry on a smooth polishing fabric. The electrode was rinsed with double distilled water and dried. Then, 2.0 μL of 0.5 mg mL^{-1} GO dispersion was dropped on the surface of the pretreated GCE and dried at an ambient temperature. Consequently, GO could be adsorbed onto the electrode. Afterward, 2.0 μL of 250 μg mL^{-1} AuNPs solution was deposited onto the surface of GO/GCE. At this stage, an AuNPs/GO thin film was formed at room temperature. Next, the AuNPs/GO/GCE surface was dried at room temperature, and then 2.5 μL droplet of an immobilization buffer solution containing 10.0 nM *H. pylori* probe (ssDNA) was placed on the AuNPs/GO/GCE surface for probe self-assembly. The self-assembly of the probe was performed by incubating the electrode at room temperature (25 ± 1 °C) for 80 min in a high-humidity container to hinder evaporation. Later, the *H. pylori* self-assembled electrode (ssDNA/AuNPs/GO/GCE) was washed with a washing solution and incubated in a 1.0 mM solution of MCH for 5 min. The electrode was rinsed with 80:20 (*v*/*v*) ethanol: water and then distilled water. The hybridization was performed by immersing the ssDNA/AuNPs-GO-GCE into a hybridization buffer solution (pH 7.0) containing 1.0 nM of the target oligonucleotide (complementary, mismatch or noncomplementary strands) at room temperature (25 ± 1 °C) for 120 min. The detailed process of biosensor fabrication is representing in the Scheme 1.

2.4. OB accumulation on the modified electrode

OB was accumulated on the ssDNA/AuNPs/GO/GCE by immersing the modified electrode into a 0.1 mM phosphate buffer solution (pH 7.0) containing 0.1 mM of OB without applying any potential to the electrode, when the mentioned solution gently stirred at 100 rpm for 100 min. Afterward, the prepared electrode was rinsed with a washing solution for 10 s. A similar procedure was applied for the accumulation of OB on a probe modified GCE which is hybridized with desired oligonucleotide samples (non-complementary, mismatch and complementary).

2.5. Voltammetric measurements

Electrochemical measurements were performed by differential pulse voltammetry (DPV), with an amplitude of 25 mV, a step potential of 50 mV, in a 0.1 M phosphate buffer solution (pH 7.0) and at a modulation time of 0.05 s. The raw data were processed with the Savitzky and Golay filter (level 2) followed by the moving average baseline correction using a peak width of 0.01. The cyclic voltammograms were plotted at a scan rate of 100 mV s^{-1}. The electrochemical impedance spectra were measured at 0.2 V from 100 kHz down to 0.01 Hz with an AC amplitude of 10 mV. All the experiments were carried out in 5 mL of 0.5 mM solution of $[Fe(CN)6]^{3-/4-}$ as a redox pair in 0.1 M PBS solution in a faraday box.

2.6. Theoretical method

In the first step, 3D structure of DNA probe was predicted using make-na web tool (http://structure.usc.edu/make-na/server.html). The resulted structure used as a receptor in molecular docking. The structural file of OB, downloaded from the ZINC database (http://zinc.docking.org/) which accession number is “zinc_4521757”. The probe and OB preparation were performed in “AutoDocktools” that including adjust Hydrogen atoms, defined atom type and add potential charge. The search space was determined by means of “Grid box plugin of AutoDocktools”. Finally molecular docking was done using vina-autodock which has more accuracy and is faster than autodock [25]. The results of docking were visualized in 2D and 3D representation using Ligplot [26] and pymol (http://www.pymol.org/) software, respectively.

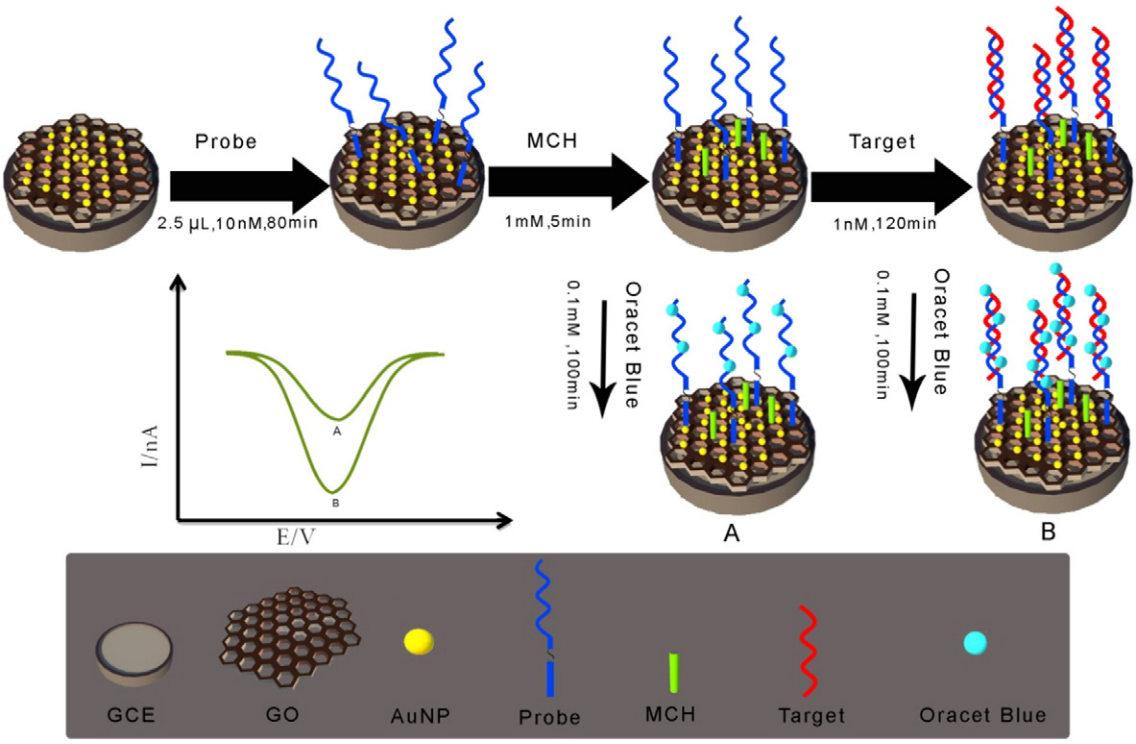

Scheme 1. Schematical fabrication process of the biosensor.

3. Results and discussion

3.1. Evaluation of the AuNPs/GO

3.1.1. Characterization of AuNPs

Characterization and specification of the AuNPs are shown by the Transmission electron microscopy (TEM) images (Fig. 1A) and UV–vis absorption spectrum (Fig. 1B). The resulted AuNPs have had satisfying uniform shape, and approximately 30 nm diameter.

3.1.2. Scanning electron microscopy analysis

The morphologies of GO, and AuNPs/GO films were evaluated by SEM (Fig. 1C and D). As can be seen from Fig. 1C, the SEM image of GO showed a planar sheet-like structure which is successfully expanded the electrode surface. After addition of the AuNPs on the surface of the GO, many pearl-like particles with diameter of ~30 nm distributed relatively uniformly onto the GO matrix (Fig. 1D).

3.2. Docking result

The binding affinity of OB for 9 clusters summarized in Table 1 which shows the binding energy for dsDNA is −8.6 kcal mol^{-1}. During the docking many different conformations were generated which grouped in 9 clusters based on RMSD. However, binding energy of this interaction for single strand is −4.9 kcal mol^{-1} (Fig. 2A). The location of binding is major/minor groove (Fig. 2B). The binding pocket has shown that the planner ring of ligand has parallel orientation with nucleotide therefore could has stacking binding with them (Fig. 2C).

The 2D representation of binding pocket was shown in (Fig. 2D) that including following nucleotide in binding with ligand. a9, a11, t9, t10, a12, g11, a10, c12. In Addition, the molecular rendering of the OB is shown in Fig. 2E. The results indicate the OB has the most effective interaction with ds-DNA rather than ss-DNA, and in the course of an experiment too. In fact the theoretical and experimental results confirmed each other.

3.3. Self-assembly of the ssDNA on AuNPs/GO/GCE

The ssDNA was immobilized using two different methods namely droplet and solution methods. In droplet self-assembly, a 2.5 μL droplet of an *H. pylori* probe solution (10.0 nM) was dropped onto the AuNPs/GO/GCE. In the second method, the AuNPs/GO/GCE was immersed in an immobilization buffer containing a 10.0 nM probe solution for 80 min. Then, both of the prepared electrodes were soaked first in MCH and subsequently in the OB solution. Similarly, OB was accumulated on the double strand DNA (dsDNA) modified electrode, and the probe self-assembled AuNPs/GO/GCE was immersed in the target DNA solution and then in the OB solution. Fig. 3A illustrates the differential pulse voltammograms (DPVs) of the OB accumulated on the surface of the ssDNA/AuNPs/GO/GCE before (curves a and b) and after hybridization with the complementary DNA (curves c and d) using the prepared electrodes through the droplet method (curves b and d) and the solution self-assembly method (curves a and c).

As illustrated, the current response of the OB accumulated on the ssDNA/AuNPs/GO/GCE prepared by the droplet method (curve b) is higher than the ones obtained from the solution method (curve a). Besides, the results demonstrate that after the hybridization process, the current response obtained from the first method (curve d) is larger than that taken from the solution method (curve c), suggesting that the probe molecules are better self-assembled by the droplet method. The fabrication steps of the ssDNA/AuNPs/GO/GCE and the dsDNA/AuNPs/GO/GCE as well as their interaction with OB label.

Fig. 3B shows the results of DPV measurements related to the OB accumulated on the ssDNA/AuNPs/GO/GCE versus the concentration of the probe. As it can be seen, the current response of the accumulated OB increased as the probe concentration is around 10.0 nM and then slightly decreased with the increase of the probe concentration. This is in agreement with the findings of Nasirizadeh et al. [20]. In that manuscript a massive accumulation of the probe on the electrode results in less availability of OB to DNA.

Fig. 3C exhibits the current response of the accumulated OB on the ssDNA/AuNPs/GO/GCE versus the required time for the probe self-

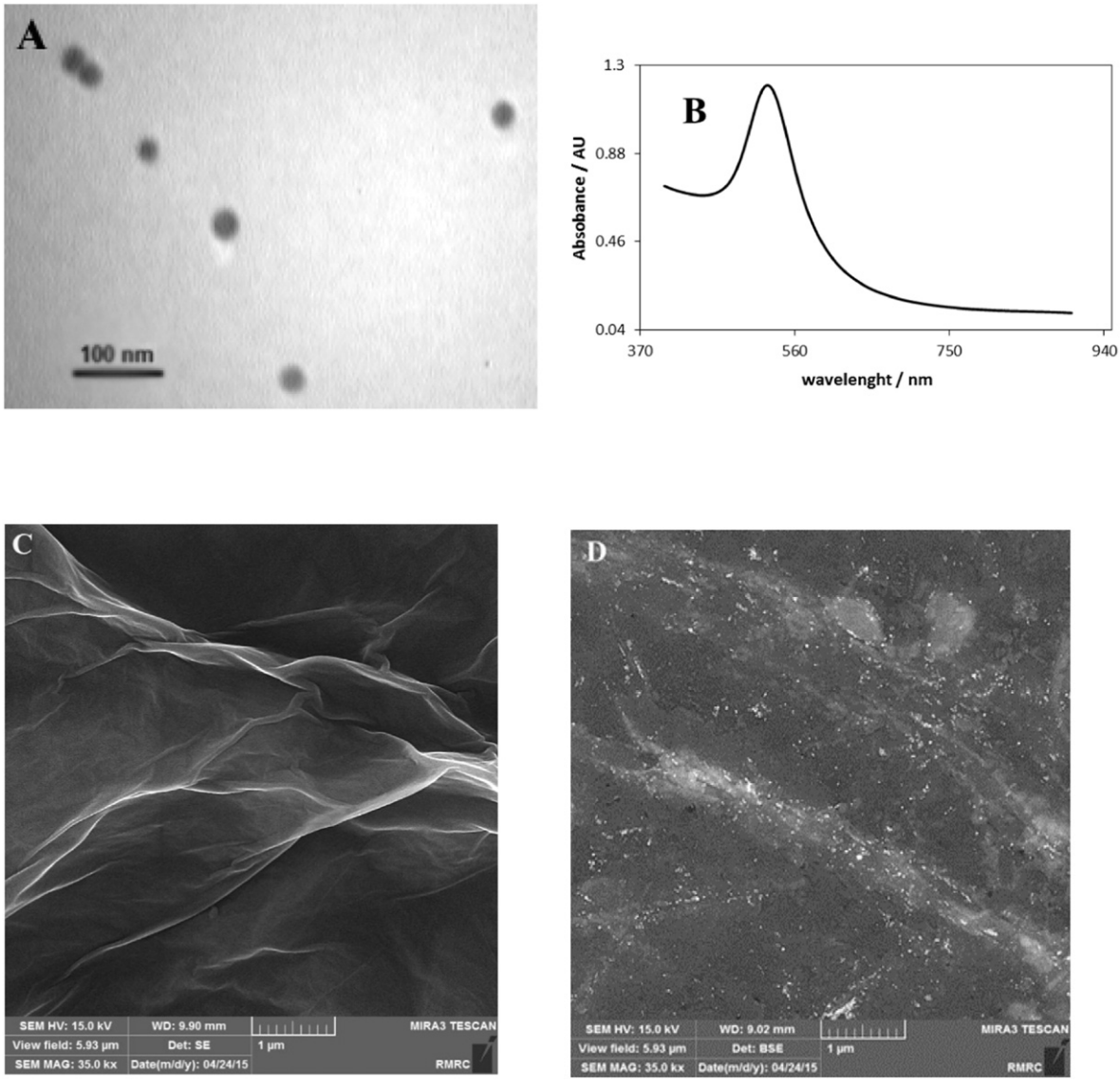

Fig. 1. The TEM image (A), Spectrophotometric analysis (B) of the AuNPs., and SEM images of GO/GCE (C) and AuNPs/GO/GCE (D).

assembly. The results showed that the accumulated OB current response was enhanced by the increase of the time of the probe immobilization up to about 80 min and then slightly decreased after 80 min. This may be happening because the electrode surface was thoroughly covered by the DNA probe after 80 min. Therefore, duration of 80 min was chosen for the probe immobilization in the subsequent experiments.

Table 1
Binding affinity of OB dsDNA.

Mode	Affinity (kcal/mol)	Distance from best mode	
		rmsd l.b.	rmsd u.b.
1	−8.6	0.000	0.000
2	−8.5	3.551	7.741
3	−8.4	12.177	16.446
4	−8.1	7.857	12.451
5	−8.1	6.117	9.335
6	−8.0	2.411	3.941
7	−8.0	2.833	4.699
8	−8.0	11.921	16.557
9	−7.9	18.408	22.232

As shown, a similar trend is observed in both experiments of the probe concentration and the self-assembly time, whereupon it can be explained that the electrode surface has a certain capacity for accumulation of DNA probe. Based on the obtained results, 10.0 nM of thiolated DNA was selected as an optimum concentration for the immobilization of the ssDNA on the AuNPs/GO/GCE.

3.4. Optimization of the hybridization process

Three different methods were employed for DNA hybridization, and their results were compared together. In the first method, referred to as the droplet method, the hybridization process was conducted by depositing a 2.5 µL droplet of a complementary solution onto the ssDNA/AuNPs/GO/GCE. To avoid evaporation, it was incubated in a high-humidity container at room temperature for 2.0 h. Finally, the modified electrode was rinsed thoroughly in a washing solution through 100-rpm stirring, and then OB was accumulated on the modified electrode surface. The DPV diagram of the accumulated OB on this electrode surface is shown in Fig. 4 curve a. In the second method, known as the preheated solution hybridization method, the ssDNA/AuNPs/GO/GCE was soaked in the hybridization solution at 85 °C for 3 min while the solution was being moderately stirred. Then, the solution was cooled

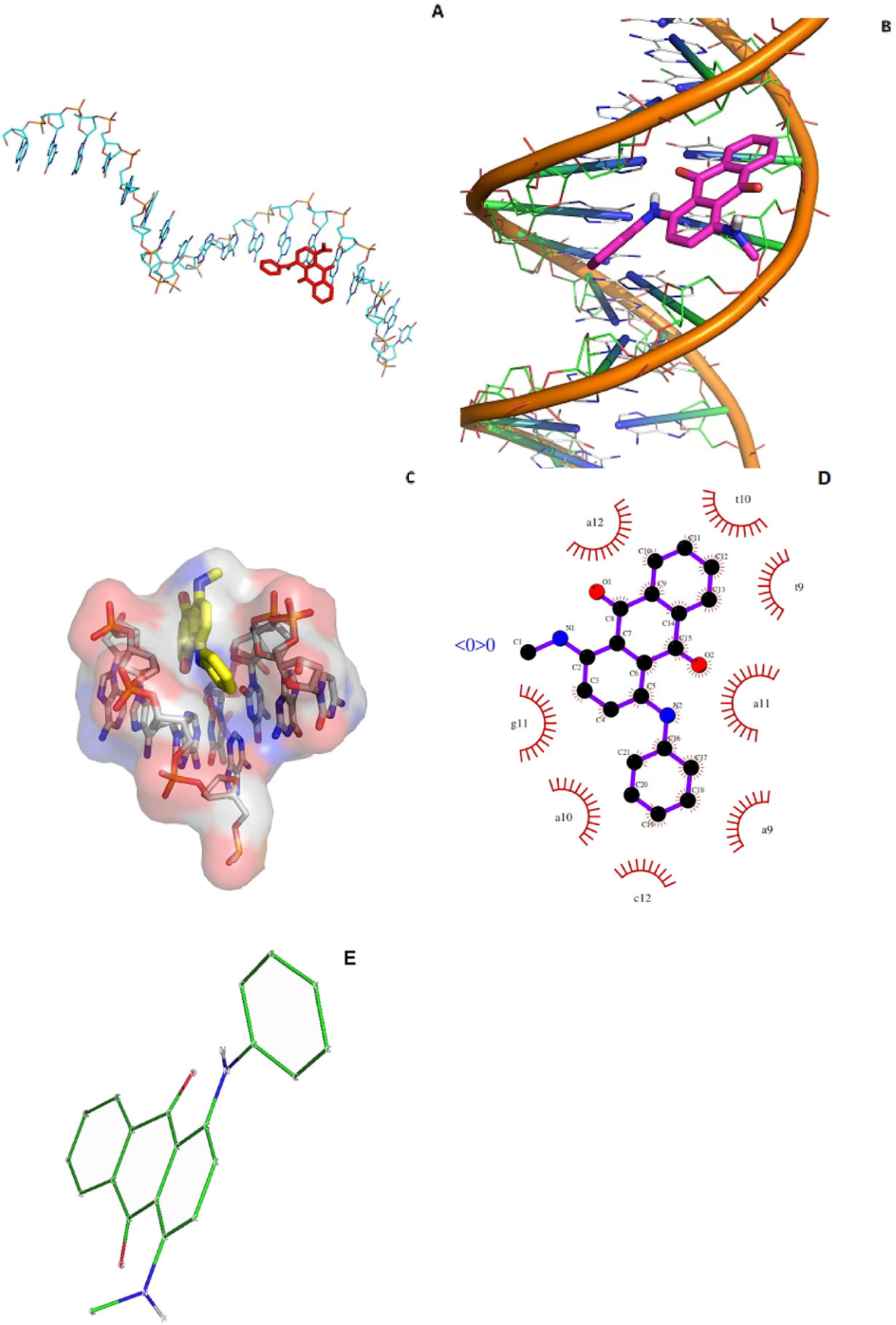

Fig. 2. A. interaction of single strand DNA with ligand. B. The location of binding is major/minor groove. C. planner ring of ligand has parallel orientation with nucleotide. D. nucleotide in binding with ligand. E: Molecular rendering of the OB.

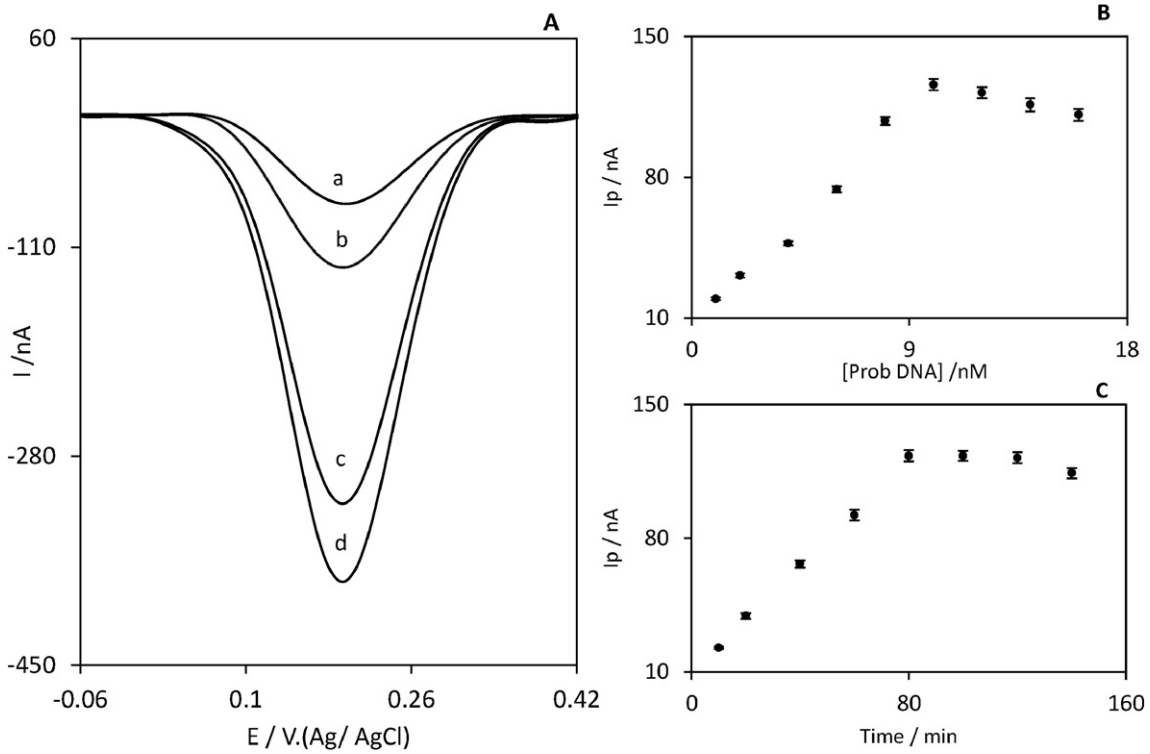

Fig. 3. (A) DPVs of the OB accumulated on the surface of ssDNA/AuNPs/GO/GCE before (voltammograms a and b) and after hybridization with the complementary DNA (voltammograms c and d) using the electrodes prepared with two different methods of the droplet self–assembly (voltammograms b and d) and the solution self-assembly (voltammograms a and c). The accumulated OB current response on ss–DNA/AuE versus (B) the consumed time for the probe self–assembly, (C) the probe concentration.

down gradually at room temperature. The electrode was rinsed with a washing solution and the OB was accumulated on the electrode. Fig. 4, curve b, presents the DPV of the accumulated OB by the preheated solution hybridization method. The third method was the solution hybridization method, practiced in the same way as the method described in Section 2.3. After hybridization, the modified electrode was immersed in the OB solution. Fig. 4, curve c, illustrates the current peak of the modified electrode by the solution method. As indicated, the highest current response was observed in the modified electrode with the solution method.

It can be said that, by the solution method, the target DNA has a good chance to gain the best orientation for hybridization. According to Fig. 4 the solution hybridization method is suggested as an optimal procedure for the hybridization process.

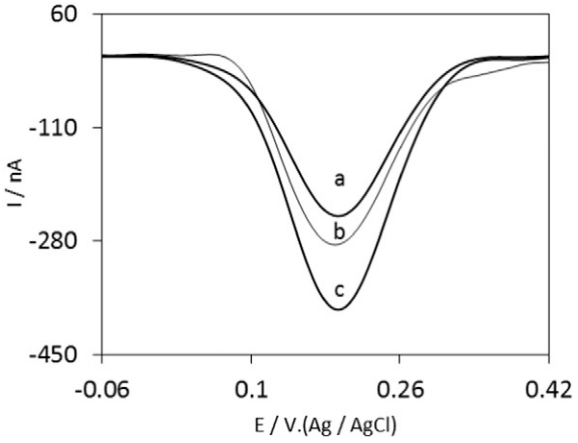

Fig. 4. DPVs of OB accumulated on the surface of dsDNA/SAM that was prepared with different hybridization methods of (a) the drop hybridization, (b) the preheated solution hybridization and (c) the solution hybridization.

3.5. Optimization of OB concentration on the modified electrode surface with dsDNA

We attempted to find out the best concentration of OB as an electroactive label on modified electrode with dsDNA. Thus, after the hybridization process, the modified GC electrode was immersed in different concentrations of OB for 100 min. Fig. 5A shows the accumulated OB signals after immersing the dsDNA/AuNPs/GO/GCE in different concentrations of OB. As presented, the signals were enhanced with the increase of OB concentration. Analytical characteristics could further increase the concentration of electroactive species at the surface of the modified electrode.

The highest cathodic current was observed at the concentration of 0.1 mM of OB (Fig. 5B), but then it remained relatively constant. So, this value was considered as the optimal concentration of the buffer solution containing OB. In addition, the effect of the accumulation time of OB was investigated. Based on the results given in Fig. 5C, the best time for accumulation of OB on the dsDNA/SAM was 100 min.

3.6. Characterization by cyclic voltammetry

Fig. 6A shows the cyclic voltammograms of the electrode in 0.5 mM $[Fe(CN)6]^{3-/4-}$ in 0.1 M KCl for GCE bare electrode, GCE/GO, AuNPs/GO/GCE, ssDNA/AuNPs/GO/GCE, MCH/ssDNA/AuNPs/GO/GCE and dsDNA/AuNPs/GO/GCE. In comparison to the performance of the bare GCE, the modified GCE/GO has a lower peak current, but the AuNPs/GO/GCE displayed a significant increase in peak current. The decrement of the current by addition of the GO, is because of the negative charge of the GO in solution which is interacting with $[Fe(CN)_6]^{3-/4-}$ ions due to the ionized functional groups, or the GO acted as an insulating layer, which have been reported in publications before [27,28]. In fact, this increase in oxidation/reduction peak current of $[Fe(CN)6]^{3-/4-}$ anions demonstrate the important role of AuNPs in obtaining higher

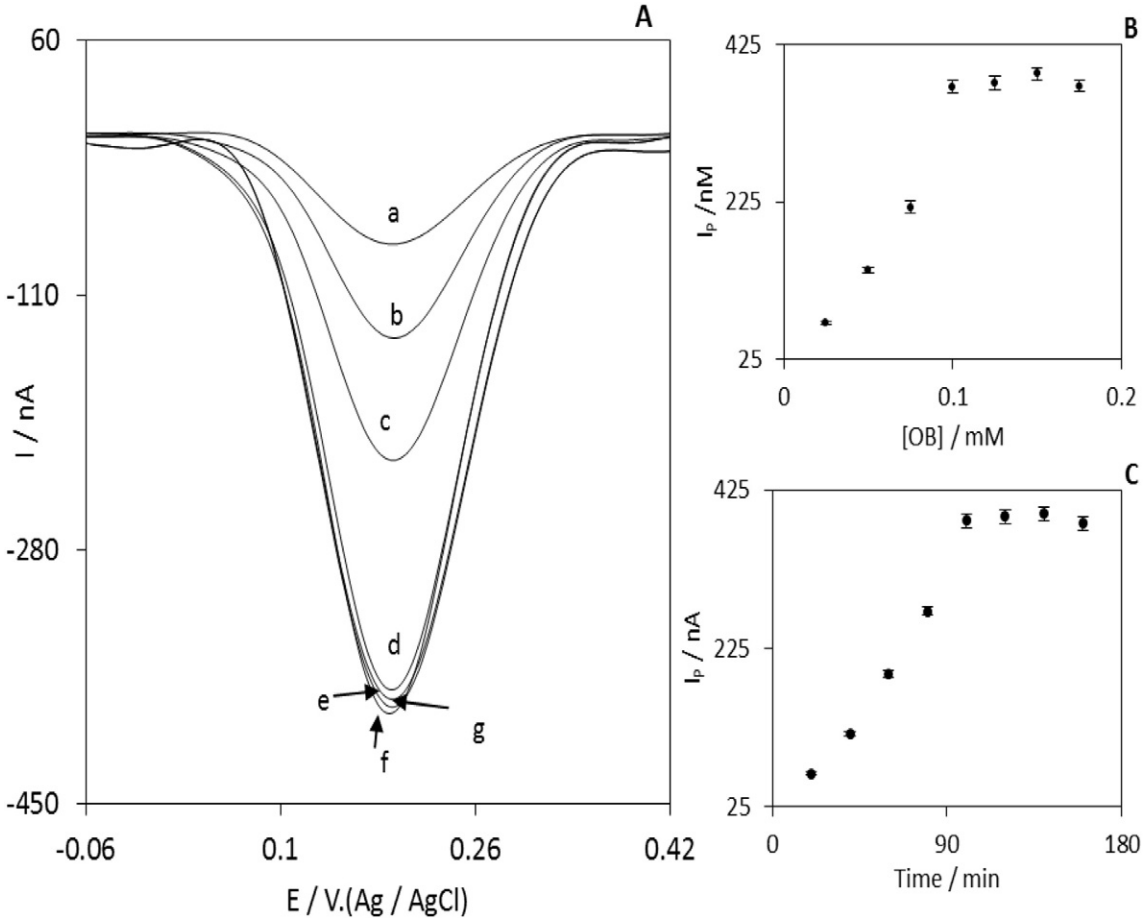

Fig. 5. (A) Differential voltammogram of the accumulated OB current response on dsDNA/AuNPs/GO/GCE versus different OB concentrations. (B) Current range versus concentration for the accumulated OB. (C) Current range versus consumed time for the accumulated OB.

electrochemical signals. This phenomenon verifies that the AuNPs not only enhances the electrode response, but also serves as active binding sites for oligonucleotide probes by providing a larger effective surface area. Binding of ssDNA onto the AuNPs/GO/GCE surface, resulting a decrease in peak current, but the MCH treatment helps the decoration of the ssDNAs on the AuNPs, therefore the current slightly increased. Following hybridization of the DNA probe with the complementary DNA, the redox peak currents decreases due to the phosphate backbone of the DNA develops more negative charges on the surface electrode. These observations confirmed the assembling procedures of the modified electrodes in every stage of biosensor preparation.

3.7. Characterization by electrochemical impedance spectroscopy

To reconfirm the CV experiments, the EIS experiments were also performed which is shown in the Fig. 6B with plots of the modified

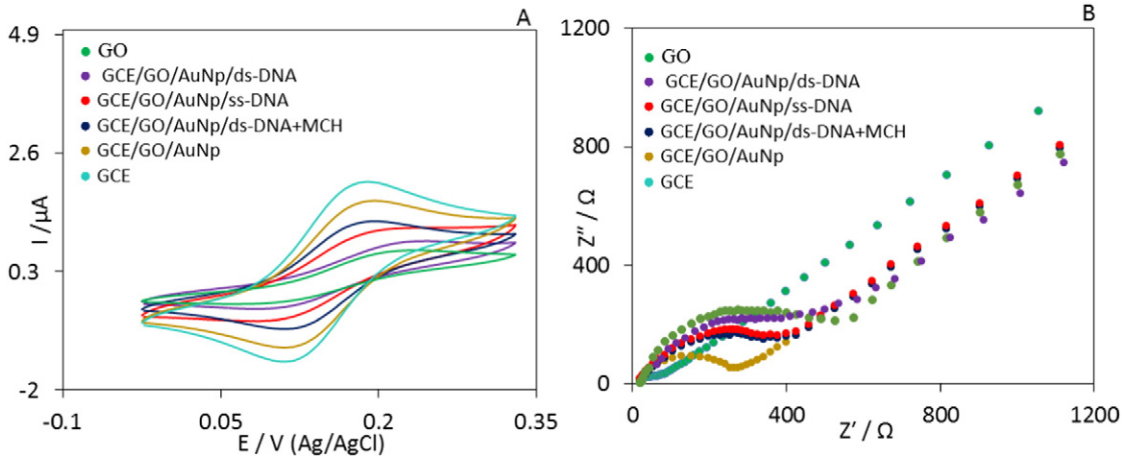

Fig. 6. A. Cyclic voltammograms of the electrode in 0.5 mM $[Fe(CN)6]^{3-/4-}$ in 0.1 M KCl for GCE bare electrode, GCE/GO, AuNPs/GO/GCE, ssDNA/AuNPs/GO/GCE, MCH/ssDNA/AuNPs/GO/GCE and dsDNA/AuNPs/GO/GCE. B. electrochemical impedance spectroscopy of the electrode in 0.5 mM $[Fe(CN)6]^{3-/4-}$ in 0.1 M KCl for GCE bare electrode, GCE/GO, AuNPs/GO/GCE, ssDNA/AuNPs/GO/GCE, MCH/ssDNA/AuNPs/GO/GCE and dsDNA/AuNPs/GO/GCE.

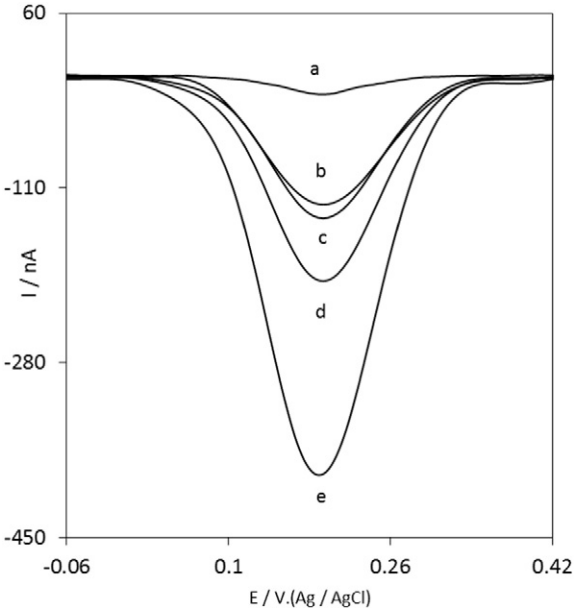

Fig. 7. DPVs of OB accumulated on the (a) MCH modified AuNPs/GO/GCE, ssDNA/AuNPs/GO/GCE before (b) and after hybridization with a 1.0 nM oligonucleotide solution of the (c) non–complementary, (d) mismatch and (e) complementary in a 0.1 M phosphate buffer solution (pH 7.0).

electrodes after each modification step. It is clearly noticeable that the bare GCE exhibits a small charge transfer resistance but for the GO modified electrode, the R_{ct} significantly increased to 517 Ω. For the AuNPs/GO/GCE reducing of the R_{ct} happened to 243 Ω because of the higher surface area and excellent conductivity of AuNPs. After immobilization of ssDNA on the AuNPs/GO/GCE, the charge transfer resistance increased to 348 Ω, because the quantity of the negative charge on the electrode surface increased greatly and the electrode surface will be relatively blocked. Upon the addition of the MCH to the ssDNA/AuNPs/GO/GCE, the assembly of the ssDNAs on the AuNPs was corrected, therefore the R_{ct} slightly decreased to 401 Ω. By hybridization of dsDNA, R_{ct} was increased to 405 Ω. Because of more repulsion between negative charge of $[Fe(CN)_6]^{3-/4-}$ and DNA phosphate groups negative charges. These results clearly supported the observations of CV experiments and reconfirmed the assembling procedure of the modified electrodes.

3.8. Analytical performance of the DNA biosensor

The selectivity of DNA hybridization on the GCE with probe DNA was evaluated by hybridizing it with its complementary sequence, mismatch sequence, and non-complementary sequence. Fig. 7 shows the DPVs of OB accumulated on the MCH modified GCE (curve a), ssDNA/AuNPs/GO/GCE before hybridization (curve b) and after hybridization with a 1.0 nM solution of non-complementary (curve c), mismatch (curve d) and complementary (curve e) oligonucleotides.

As shown in Fig. 7, in comparison to the DPV response of OB with the ssDNA modified GCE (curve b), an increase was observed in the peak current value of OB when the DNA probe was hybridized with its complementary sequence (curve e). The current peak obtained by probe hybridization with the mismatch DNA (curve d) was higher than the one with the non-complementary sequence (curve c). The results showed that the modified electrode had satisfactory selectivity for DNA hybridization.

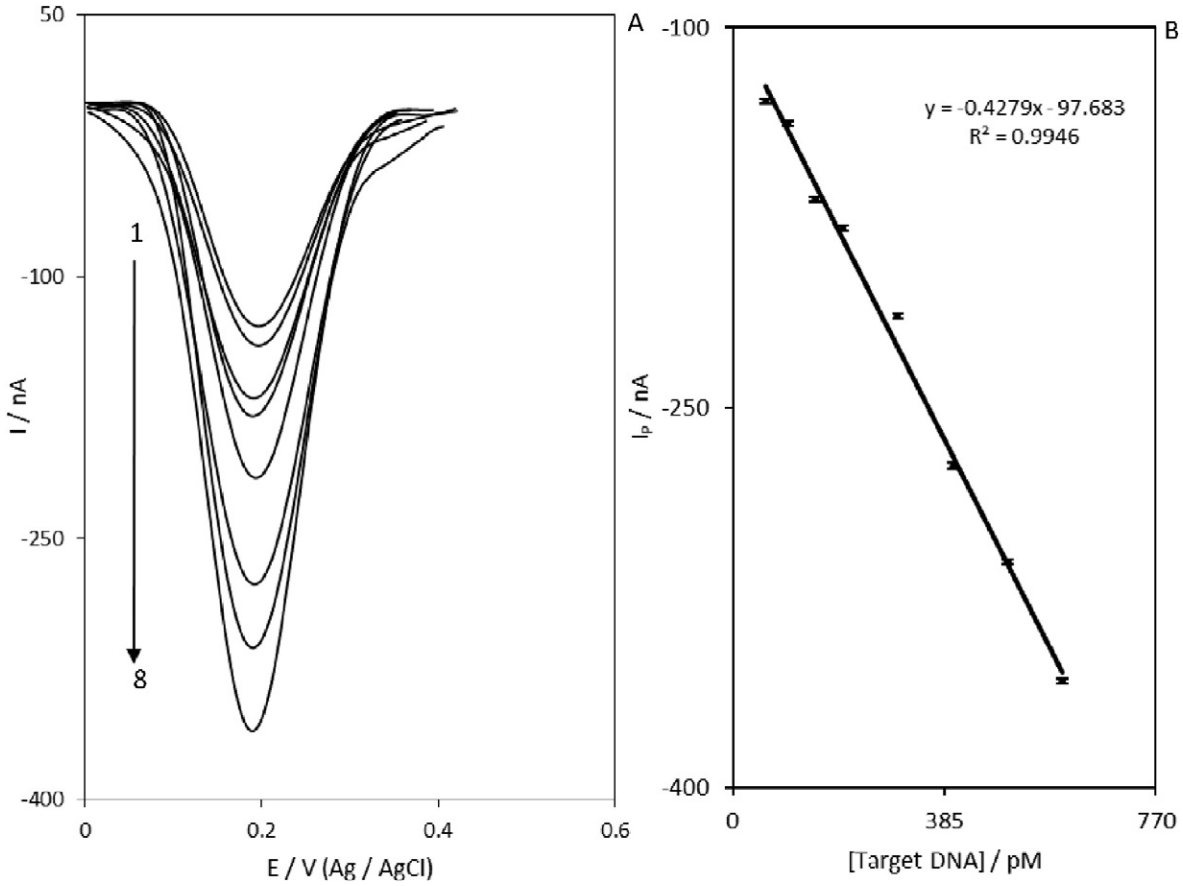

Fig. 8. (A) DPVs of OB accumulated on the hybridized ssDNA/AuNPs/GO/GCE with different concentrations of the complementary (target) DNA in a 0.1 M phosphate buffer solution (pH 7.0). The numbers of 1–11 correspond to 60–600 pM target DNA. Inset (B) shows the plot of difference in the accumulated OB current response on ds–DNA/AuE and ss–DNA/SAM ($\Delta I = I_{ds-DNA} - I_{ss-DNA}$) versus the target DNA concentration in the hybridization process.

Table 2
Comparison of the analytical parameters of different biosensors for DNA determination.

Electroactive indicator	Linear range (pM)	Detection limit (pM)	Electrochemical method	Sensitivity (nA pM^{-1})	Mismatch detection	Electrode	Ref.
Hematoxylin	1.25×10^4–3.5×10^5	3.8×10^3	DPV	1.14×10^{-9}	Single-base mismatch	Gold electrode	[20]
Methylene blue	2.0×10^3–1.0×10^4	1.49×10^3	DPV	0.78×10^{-3}	–	Pencil graphite	[29]
ZnO nanowires	1.0×10^7–1.0×10^8	3.32×10^6	DPV	6.36×10^{-3}	–	Gold electrode	[30]
Methylene blue	5.0×10^4–1.0×10^8	3.6×10^4	CV	1.10×10^{-9}	–	Gold electrode	[31]
Methylene blue	5.0×10^3–1.0×10^5	4.35×10^3	DPV	0.53×10^{-2}	–	Gold electrode	[32]
Anthraquinone	2.0×10^4–1.2×10^7	4.0×10^3	DPV	0.28×10^{-3}	–	Screen-printed carbon electrode	[33]
Methylene blue	1.87×10^4–2.50×10^5	1.81×10^4	DPV	0.32×10^{-2}	–	Gold electrode	[34]
$[Ru(phen)3]^{2+}$	0.1–100	0.04	DPV	2.22×10^{-9}	–	Glassy carbon electrode	[19]
Methylene blue	1.0×10^{-3}–5.0	3.8×10^{-4}	DPV	0.30×10^{-9}	–	Gold electrode	[35]
Methylene blue	1.0×10^{-1}–1.0×10^6	3.12×10^{-2}	DPV	4.11×10^{-9}	Single-base mismatch	Carbon ionic liquid electrode	[36]
Gold(I) complexes	1.0×10^3–2×10^4	0.5×10^3	CV	8.25×10^3		Glassy carbon electrode	[37]
Methylene blue	2.5×10^4–1.0×10^5	0.2×10^3	CV	–	Single-base mismatch	Gold electrode	[38]
Carboxylic group functionalized SWCNTs	4.0×10^4–1.1×10^5	2.0×10^4	DPV	0.17×10^{-1}	Single-base mismatch	Glassy carbon electrode	[39]
OB	60.0–600.0	27	DPV	0.42	Single-base mismatch	glassy carbon electrode	This work

Fig. 8A displays the DPV hybridization responses for increase of the target concentrations of the complementary sequence from 60 pM to 600 pM. The peak current of the accumulated OB was increased with the increment of the complementary target DNA concentrations, and it has a linear relationship with the value of the complementary target DNA concentrations, as shown in the Fig. 8B. The linear regression equation was $y = -0.4279 \times -97.683$ with a correlation coefficient value of 0.9946 (x is the concentration of the complementary sequence and y is the consequent peak current). The calibration plot, in the range of 60.0–600.0 pM of the target DNA, was used to estimate the lower limit of the target DNA detection at the ssDNA/AuNPs/GO/GCE. The lower detection limit, Cm and limit of quantification (LOQ) were found to be 27.0 pM and 90.0 pM, by using the equation $Cm = 3s_{bl}/m$ and $LOQ = 10s_{bl}/m$, where s_{bl} is the standard deviation of the blank response (nA) and m is the slope of the calibration plot (-0.4279 nA nM^{-1}). The average voltammetric current and the precision estimated in terms of the relative standard deviation (RSD) for twelve repeated measurements ($n = 12$) of 150.0 pM of the target DNA were 168.0 ± 5.7 nA and 3.4% respectively. In addition, the response time of prepared electrode is about 220 min which is lower than the majority of the previous publications. In Table 2, some of the analytical characteristics obtained in this study are compared with those previously reported by others [20, 29–40]. As it can be seen, some analytical responses such as detection limit and linear range of response are higher in some cases versus represented works in Table 2. Therefore the represented biosensor has relative better response than other previously published DNA biosensors, especially in response time, sensitivity and selectivity.

In order to study the stability of the modified electrodes, the AuNPs/GO/GCE modified electrodes which were immobilized by ssDNA have been produced with the method described in the experimental part Section 2.3; and have been kept for different time periods (days) in temperature of 4 °C in the phosphate buffer solution pH 7.0. The aforementioned modified electrodes were examined for the purpose of the measurement target DNA sample, in the temporal range of 1 to 14 days. The results have shown that the modified electrodes have the best stability for less than 3 days, and after 3 days, the OB decomposition placed on the ss-DNA show more than 5% decrease. In conclusion, the best stability of the electrodes immobilized by ssDNA is within 3 days storage under the temperature of 4 °C, for the most effective use in measurements.

3.9. Study of chemical interferences on DNA hybridization

To evaluate the effect of candidate interferences on the proposed biosensing platform, different chemicals have been studied, including cetyltrimethyl ammonium bromide (CTAB), sodium dodecyl sulfate (SDS), ethanol, chloroform and glucose [40]. Aforementioned chemicals have added to the hybridization buffer up to 1% final concentration. The hybridization of the ss-DNA on the electrode with the target DNA (110.0 pM) was carried out and the DPVs were performed which is shown in the Fig. 9. As it can be seen, the presences of these potential interferences have not any significant effect on the hybridization process of the proposed biosensor. Furthermore, the specificity and selectivity of the proposed system and also the low potential reduction peak of the label provide additional insurance to reconfirm the proposed DNA biosensor.

3.10. Real sample evaluation

To evaluate the functionality of the proposed biosensor in real sample environment, the extracted DNA solution was simulated using four potential interferences which could possibly found in the extracted bacterial DNA. To perform this experiment, the target DNA solution was spiked with the solution containing the combination of the four potential interferences including 0.25% SDS, 0.25% ethanol, 0.25% glucose and 0.25% CTAB [40]. The results showed that the mentioned reagents do not have any interferences in the determination of our target because in our determination potential range these reagents do not displays electroactive role. Table 3 representing the real sample analysis for four different concentrations in the linear range, with their recovery

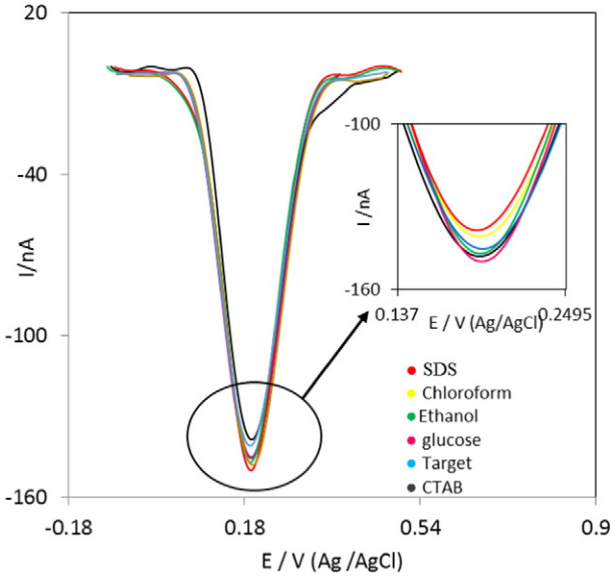

Fig. 9. Effect of candidate interferences on proposed biosensing platform, including CTAB, SDS, ethanol, chloroform and glucose.

Table 3
The real sample results of the proposed biosensor.

Sample	Spiked (pM)	Detected (pM)	Recovery (%)	RSD (%)
1	10	9.72	97.2	3.7
2	20	19.6	98.0	2.9
3	40	41.0	102.5	2.4
4	80	78.7	98.4	2.1

percentages and RSD. As it is shown, high recovery percentages with very low RSD percentages are representing the potential application of the proposed biosensor to be used in future clinical sample analysis.

4. Conclusion

In this study, the interactions of OB were investigated as an electroactive DNA label. Different affinities of OB were employed to ssDNA and dsDNA for the development of a DNA biosensor for the purpose of detecting and discriminating *H. pylori* corresponding to oligonucleotide from non-complementary DNA. The experiments also confirmed that OB-based DNA biosensors are capable of detecting the single-base mismatch in the target DNA. The study has provided evidence that the best method for probe self-assembly is drop self-assembly and the best hybridization method is solution hybridization. Under optimum conditions, electrical signals have a linear relationship with the concentration of the target DNA ranging from 60.0 pM to 600.0 pM, and the detection limit is 27.0 pM. The great responses of the biosensor in the simulated real sample, representing its potential to be used in future clinical application for *H. pylori* detection.

References

[1] N. Salama, Life in the human stomach persistence strategies of the bacterial pathogen *Helicobacter pylori*, Nat. Rev. Microbiol. 11 (6) (2013) 385–399.
[2] W. Chan, P. Hui, K.M. Leung, J. Chow, F. Kwok, Coccoid forms of *Helicobacter pylori* in the human stomach, Am. J. Clin. Pathol. 102 (4) (1994) 503–507.
[3] J. Tzeng, Y.L. Lin, S. Chung, Y. Chu, Comparison of four diagnostic methods for *Helicobacter pylori*, Tzu Chi Med. J. 17 (5) (2005) 339–343.
[4] Y. Cho, C. Kuo, S. Wang, Y. Chen, B. Weng, Y. Lee, C. Cheng, J. Shiea, D. Wu, Differentiation of virulence of *Helicobacter pylori* by matrix-assisted laser desorption/ionization mass spectrometry and multivariate analyses, Clin. Chim. Acta 424 (2013) 123–130.
[5] E. Ilina, A. Borovskaya, M. Serebryakova, V. Chelysheva, K. Momynaliev, T. Maier, M. Kostrzewa, M. Govorun, Application of matrix-assisted laser desorption/ionization time-of-flight mass spectrometry for the study of *Helicobacter pylori*, Rapid Commun. Mass Spectrom. 24 (3) (2010) 328–334.
[6] M. Wilson, R. Gray, P. Smith, F. Meister, K. Osann, C. Smith, Fluorescence diagnostics of *Helicobacter pylori*-infected human gastric mucosa: establishing technique and validity, Scand. J. Gastroenterol. 42 (8) (2007) 941–950.
[7] M. Utt, B. Danielsson, T. Wadstrom, *Helicobacter pylori* vacuolating cytotoxin binding to a putative cell surface receptor, heparan sulfate, studied by surface plasmon resonance, FEMS Immunol. Med. Microbiol. 30 (2) (2001) 109–113.
[8] M.V. del Pozo, C. Alonso, F. Pariente, E. Lorenzo, DNA biosensor for detection of *Helicobacter pylori* using phendione as the electrochemically active ligand in osmium complexes, Anal. Chem. 77 (8) (2005) 2550–2557.
[9] J.M. Whitmire, D.S. Merrell, Successful culture techniques for helicobacter species: verification of helicobacter identity using 16S rRNA gene sequence analysis, Methods Mol. Biol. 921 (2012) 37–40.
[10] E. Rimbara, M. Sasatsu, D.Y. Graham, PCR detection of *Helicobacter pylori* in clinical samples, Methods Mol. Biol. 943 (2013) 279–287.
[11] Y. Zhang, W. Jiang, Decorating graphene sheets with gold nanoparticles for the detection of sequence-specific DNA, Electrochim. Acta 71 (2012) 239–245.
[12] J. Wang, Nanomaterial-based amplified transduction of bio molecular interactions, Small 1 (11) (2005) 1036–1043.
[13] M. Pumera, Graphene in biosensing, Mater. Today 14 (7–8) (2011) 308–315.
[14] W. Sun, L. Li, B. Lei, T. Li, X. Ju, X. Wang, G. Li, Z. Sun, Fabrication of graphene–platinum nanocomposite for the direct electrochemistry and electrocatalysis of myoglobin, Mater. Sci. Eng. C 33 (2013) 1907–1913.
[15] L. Hlavata, K. Benikova, V. Vyskocil, J. Labuda, Evaluation of damage to DNA induced by UV-C radiation and chemical agents using electrochemical biosensor based on low molecular weight DNA and screen-printed carbon electrode, Electrochim. Acta 71 (2012) 134–139.
[16] S. Niu, B. Han, W. Cao, S. Zhang, Sensitive DNA biosensor improved by luteolin copper(II) as indicator based on silver nanoparticles and carbon nanotubes modified electrode, Anal. Chim. Acta 651 (2009) 42–47.
[17] Y. Zhang, J. Wang, M. Xu, A sensitive DNA biosensor fabricated with gold nanoparticles/poly (p-amino benzoic acid)/carbon nanotubes modified electrode, Colloids Surf. B 75 (1) (2010) 179–185.
[18] X. Han, X. Fang, A. Shi, J. Wang, Y. Zhang, An electrochemical DNA biosensor based on gold nanorods decorated graphene oxide sheets for sensing platform, Anal. Biochem. 443 (2) (2013) 117–123.
[19] H. Huang, W. Bai, C. Dong, R. Guo, Z. Liu, An ultrasensitive electrochemical DNA biosensor based on graphene/Au nano rod/poly thionine for human papillomavirus DNA detection, Biosens. Bioelectron. 68 (2015) 442–446.
[20] Z. Shakoori, S. Salimian, S. Kharrazi, M. Adabi, R. Saber, Electrochemical DNA biosensor based on gold nanorods for detecting hepatitis B virus, Anal. Bioanal. Chem. 407 (2) (2015) 455–461.
[21] H. Peng, Y. Hu, P. Liu, Y. Deng, P. Wang, W. Chen, A. Liu, Y. Chen, X. Lin, Label-free electrochemical DNA biosensor for rapid detection of mutidrug resistance gene based on Au nanoparticles/toluidine blue–graphene oxide nanocomposites, Sensors and Actuators B 207 (2015) 269–276.
[22] N. Nasirizadeh, H.R. Zare, M.H. Pournaghi-Azar, M.S. Hejazi, Introduction of hematoxylin as an electroactive label for DNA biosensors and its employment in detection of target DNA sequence and single-base mismatch in human papilloma virus corresponding to oligonucleotide, Biosens. Bioelectron. 26 (5) (2011) 2638–2644.
[23] H. Zare, N. Nasirizadeh, Fabrication, characterization and analytical performance of the hydroxylamine sensor based on an OB multi-walled carbon nanotubes film deposited on an electrode surface, J. Braz. Chem. Soc. 23 (6) (2012) 1070–1077.
[24] H. Zare, R. Rajabzadeh, N. Nasirizadeh, M.M. Ardakani, Voltammetric studies of an oracet blue modified glassy carbon electrode and its application for the simultaneous determination of dopamine, ascorbic acid and uric acid, J. Electroanal. Chem. 589 (1) (2006) 60–69.
[25] O. Trott, A.J. Olson, AutoDock vina: improving the speed and accuracy of docking with a new scoring function, efficient optimization and multithreading, J. Comput. Chem. 31 (2) (2010) 455–461.
[26] A. Wallace, R. Laskowski, J. Thornton, LIGPLOT: a program to generate schematic diagrams of protein-ligand interactions, Protein Eng. 8 (1996) 127–134.
[27] E. Zor, I. Hatay Patir, H. Bingol, M. Ersoz, An electrochemical biosensor based on human serum albumin/graphene oxide/3-aminopropyltriethoxysilane modified ITO electrode for the enantioselective discrimination of D- and L-tryptophan, Biosens. Bioelectron. 42 (2013) 321–325.
[28] Z. Wang, X. Zhou, J. Zhang, H. Zhang, Direct electrochemical reduction of single-layer graphene oxide and subsequent functionalization with glucose oxidase, J. Phys. Chem. C 113 (32) (2009) 14071–14075.
[29] E. Souza, G. Nascimento, N. Santana, D. Ferreira, J. Bibiano, M. Arruda, D. Bruneska, J. Filho, Electrochemical DNA biosensor for sequences related to the human papillomavirus type 16 using methylene blue, Biosens. J. 3 (2014) 107–111.
[30] N. Mansor, Z.M. Zain, H. Hamzah, M. Noorden, S. Jaapar, V. Beni, Z. Ibupoto, Detection of breast cancer 1 (BRCA1) gene using an electrochemical DNA biosensor based on immobilized ZnO nanowires, Open J. Appl. Biosens. 3 (2014) 9–17.
[31] L. Zhu, R. Zhao, K. Wang, H. Xiang, Z. Shang, W. Sun, Electrochemical behaviors of methylene blue on DNA modified electrode and its application to the detection of PCR product from NOS sequence, Sensors 8 (9) (2008) 5649–5660.
[32] G. Nascimento, E. Souza, D. Erreira, M.S. Arruda, C. Castelletti, M. Wanderley, M. Ekert, D. Bruneska, J. Filho, Electrochemical DNA biosensor for bovine papillomavirus detection using polymeric film on screen-printed electrode, Biosens. Bioelectron. 38 (1) (2012) 61–66.
[33] S. Jampasa, W. Wonsawat, N. Rodthongkum, W. Siangproh, P. Yanatatsaneejit, T. Vilaivanf, O. Chailapakul, Electrochemical detection of human papillomavirus DNA type 16 using a pyrrolidinyl peptide nucleic acid probe immobilized on screen-printed carbon electrodes, Biosens. Bioelectron. 54 (2014) 428–434.
[34] D. Campos-Ferreira, G. Nascimento, E.V. Souza, M. Souto-Maior, M.S. Arruda, D.M. Zanforlin, D. Bruneska, J.L. Lima-Filho, Electrochemical DNA biosensor for human papillomavirus 16 detection in real samples, Anal. Chim. Acta 804 (2013) 258–263.
[35] X. Zhang, F. Gao, X. Cai, M. Zheng, F. Gao, S. Jiang, Q. Wang, Application of graphene–pyrenebutyric acid nanocomposite as probe oligonucleotide immobilization platform in a DNA biosensor, Mater. Sci. Eng. C 33 (7) (2013) 3851–3857.
[36] W. Sun, X. Wang, Y. Lu, S. Gong, X. Qi, B. Lei, Z. Sun, G. Li, Electrochemical deoxyribonucleic acid biosensor based on electrodeposited graphene and nickel oxide nanoparticle modified electrode for the detection of salmonella enteritidis gene sequence, Mater. Sci. Eng. C 49 (2015) 34–39.
[37] A. Escosura-Muniz, M.B. Gonzalez-Garcia, A. Costa-Garcis, DNA hybridization sensor based on aurothiomalate electroactive label on glassy carbon electrodes, Biosens. Bioelectron. 22 (2007) 1048–1054.
[38] Y. Jin, X. Yao, Q. Liu, J. Li, Hairpin DNA probe based electrochemical biosensor using methylene blue as hybridization indicator, Biosens. Bioelectron. 22 (2007) 1126–1130.
[39] X. Zhang, K. Jiao, S. Liu, Y. Hu, Readily reusable electrochemical DNA hybridization biosensor based on the interaction of DNA with single-walled carbon nanotubes, Anal. Chem. 81 (2009) 6006–6012.
[40] W.C. Liao, M.C. Chuang, J.A. Ho, Electrochemical sensor for multiplex screening of genetically modified DNA: identification of biotechcropsbylogic-based biomolecular analysis, Biosens. Bioelectron. 50 (2013) 414–420.